Solar Phys (2020) 295:83
https://doi.org/10.1007/s11207-020-01630-2

Model Fitting of Wind Magnetic Clouds for the Period 2004 – 2006

R.P. Lepping[1] · C.-C. Wu[2] · D.B. Berdichevsky[3,4] · A. Szabo[5]

Received: 6 June 2019 / Accepted: 28 April 2020 / Published online: 22 June 2020

Abstract We give the results of parameter fitting of the magnetic clouds (MCs) observed by the Wind spacecraft for the three year period – 2004 to the end of 2006 (the "Present period") using the force-free MC model of Lepping, Jones, and Burlaga (*J. Geophys. Res.* **95**, 11957, 1990). There were 19 MCs identified in the Present period, which was mainly in the declining phase of the solar cycle. The long-term occurrence rate of MCs is 10.3/year (1995-2015), whereas the occurrence rate for the Present period is only 6.3/year, similar to that for the period 2007-2009. Hence, the MC occurrence rate has had an appreciable decrease for the six years 2004-2009. The MC modeling gives such basic MC quantities as size, axial orientation, field handedness, axial magnetic field strength, center time, and closest approach vector. A statistically based modification of the modeled field intensity is tested. Also calculated are derived quantities, such as axial magnetic flux, axial current density, and axial current. Quality (Q_0) estimates are assigned representing excellent (1), good/fair (2), and poor (3). We provide error estimates on the specific fit parameters for the individual MCs for the $Q_0 = 1, 2$ cases, and give a distribution of MC types (i.e. N $\Rightarrow$ S, S $\Rightarrow$ N, All N, All S, etc., ten categories in all). There is an inordinately large percentage of the N $\Rightarrow$ S type in the Present period (32%). The Present period basic model fitting results are compared to the results of the full Wind mission and other 3-year periods. First, we notice that during the Present period the MCs are, on average, significantly faster (by 21%), distinctly stronger in axial magnetic field (by 37%), and smaller in diameter (by 5.5%), than those in the Long-term period. The quality of the MCs in the Present period is significantly better than that of the Long-term period, where the ratio $N(Q_0 = 1, 2)/N(Q_0 = 1, 2, 3)$ for each is 0.79 and 0.58, respectively. The Present period is quite different from the Long-term period (1995-2015), it is from the other three 3-year periods between 2006 and the end of

✉ R.P. Lepping
Ronald.P.Lepping@gmail.com

1 UMBC, Baltimore, MD 21250, USA

2 Naval Research Laboratory, Washington, DC 20735, USA

3 MC 672, GSFC/NASA, Greenbelt, MD 20771, USA

4 IFIR/UNR-CONICET, Esmeralda y 27 de Febrero, 2000 Rosario, Sta Fé, Argentina

5 Heliophysics Science Division, NASA/Goddard Space Flight Center, Greenbelt, MD 20771, USA

2015. In the Present period upstream shocks occur for the first 12 MCs of the 19 cases (63%); for comparison the Long-term rate is 56%.

Keywords Magnetic clouds · Interplanetary shocks · Magnetic field · Solar wind

1. Introduction

In this study we carry out parameter fitting of the magnetic clouds (MCs) observed by the Wind spacecraft for the three year period – 2004 to the end of 2006 (which occurred mainly in a declining phase of the solar cycle), using the force-free MC model of Lepping, Jones, and Burlaga (1990) (henceforth called LJB). Similar fittings have been carried out for the period of 1995 to 2003, inclusive, and for 2007 to 2015, inclusive (in 3-year segments), so this analysis of MCs for the 2004-2006 period (henceforth called the "Present period") is an attempt to fill in a 3-year gap. The primary results comprise estimates of the basic parameters defining the MCs (with uncertainties), as well as estimates of second order quantities, such as axial magnetic flux, total axial current density, and total axial current. Quality (Q_0) is estimated for each MC where $Q_0 = 1, 2, 3$ represents excellent, good/fair, and poor, respectively; see Appendix C for a definition of quality. For the $Q_0 = 1, 2$ subset we provide error estimates on the specific fit parameters for the individual MCs. Also in this study MC Type (where $B_{Z,GSE}$ is one of: All S, All N, N $\Rightarrow$ S, S $\Rightarrow$ N, etc., determined visually) will be assigned to each MC and the occurrence distribution displayed. MC Type is important in itself (especially with regard to the MC relationship to its solar origin), but it is also of key importance when the MC-geomagnetosphere interaction and magnetic storms are considered. All of the displayed MC quantities, that are based on the time period of interest (2004-2006), are on average compared to the results of the full Wind mission of 1995 to the end of 2015, and are also compared to the results of the MC fitting of cases for the three periods 2007- 2009, 2010-2012, and 2013-2015, separately. Also shock waves upstream of the present set of MCs are identified and listed. The definition of an interplanetary (IP) MC used here is given in detail by Lepping et al. (2018a), also see Burlaga et al. (1981), Klein and Burlaga (1982), Burlaga (1988, 1995). MCs are also known to be large structures, e.g. see Marubashi (1997), Lepping et al. (2018a, in Table 4), with durations that are between about 7 and 40 hours at 1 AU. That feature is retained as part of our definition. As we will see, the present 3-year period of interest is unique in many respects, providing only a small number of events, but on average of quite good quality, having strong axial field strength, being fast moving (at least several of them), and having high axial magnetic flux.

MCs can be thought of as a special class of solar ejecta usually with magnetic flux rope configurations; see Burlaga (1995), who puts MCs in proper perspective, and Dryer (1994), who reviews solar wind disturbances generally, including MCs. Also see Priest (1990) who discusses the equilibrium of magnetic flux ropes and Berdichevsky (2013) who studies the magnetic fields and mass constraints for the uniform propagation of magnetic flux ropes undergoing isotropic expansion. Examples of other MC fitting models with a greater numbers of fitting parameters than the LJB model are described by Vandas, Fisher, and Geranios (1991), Hidalgo, Nieves-Chinchilla, and Cid (2002), Vandas, Romashets, and Watari (2005), Marubashi and Lepping (2007), Wang et al. (2015), Vandas and Romashets (2017), and Nieves-Chinchilla (2018), Nieves-Chinchilla et al. (2018a,b). See Li, Luhmann, and Lynch (2018) on the solar cycle dependence and sources of MCs, and Vršnak et al. (2019) on the heliospheric evolution of MCs. Also see Wei et al. (2003) and Zhou et al. (2019) on aspects of the boundary layers of MCs, in particular on their identification and heating, respectively.

For further historical background on the study of MCs generally see Chapter 6 in Burlaga (1995) and the introduction to Lepping et al. (2018a).

This article has the following outline (section number): (1) Introduction, (2) Results for the Years 2004-2006, (3) Statistically Modified Field Intensity Within MCs, (4) Comparisons of Results to Those of Earlier and Later Periods, (5) Magnetic Cloud Type, (6) Upstream Shock Waves, and (7) Summary and Discussion.

2. Results for the Years 2004-2006, the Present Period

This work helps to provide a more comprehensive and complete presentation of the LJB model-estimated parameters of Wind MCs than are listed at the world wide website (WWW) to the date this article was submitted. That is, this work fills a gap for the years 2004-2006, so that a complete set of MC fit parameters and related derived quantities starting near the Wind launch until the end of 2015 are now given at the Wind/Magnetic Field Investigation (MFI) instrument website:

http://lepmfi.gsfc.nasa.gov/mfi/mag_cloud_pub1.html.

Especially see an updated Table 2 at that site (Summary of MC parameters). Other tables listed under this URL are of direct interest also, such as those on the MC closest approach vectors and related uncertainties for the fit parameters, described by Lepping et al. (2006) and covering the years 1995-2003, and later publications on MCs from the year 2007 up to and including 2015 (see Lepping et al., 2011, 2015, 2018a) in 3-year segments each. Also the work described here in Section 3, modification of the MC magnitudes, are added to this site.

Lepping, Wu, and Berdichevsky (2005) describe a computer (Auto-ID) program that was developed to automatically identify MCs. That program and a comprehensive visual inspection of the relevant data have been used for the identification of the Present period Wind MCs that are discussed here, as we have done for all other Wind MCs studied since the development of the Auto-ID program in 2004. When the program finds a candidate MC event, the MC magnetic field and average plasma speed are submitted as input to the LJB MC model program for least-squares parameter fitting, as described in Appendix A. If a candidate MC event cannot be fitted by this program (and there are a variety of reasons why this may happen), we refer to it as a MC-like (MCL) event. We maintain a listing of MCL events on the Wind/ MFI website, just as we do for actual MC events. See Wu and Lepping (2015) on a comparison of MC and MCL events for the period 1995-2012.

Table 1 shows a summary of the results of the fitting of MCs in the Present period (2004-2006). There is a relatively small number of MCs (N(total) = 19) in these three years when compared to most of the 3-year periods of the Wind mission; this is especially so since the year 2006. There is only N($Q_0 = 1$) = 1 case in the Present period. There are N($Q_0 = 2$) = 14 cases, and only N($Q_0 = 3$) = 4 cases so $Q_0 = 2$ cases clearly dominate. When cases $Q_0 = 1, 2$ are combined and compared to the total number of cases for each 3-year period since the year 2006, it is found that they clearly dominate in percentage (79%), as well as does the Long-term period percentage of $Q_0 = 1, 2$ cases which is 58% (see Table 4).

Figure 1 illustrates with histograms the 16 principal quantities of interest for the Present period, including the seven fundamental fit parameters listed below (i.e. B_0, H, $2R_0$, φ_A, θ_A, t_0 (or asf), and Y_0 (or *CA*)) and the six derived quantities (J_0, Φ_0, I_T, R_T, β_{CA}, *Check*) given by Equations 10 through 15, as well as the average field components in cloud (Cl) coordinates; see Figure 2 and Appendix B, which defines Cl coordinates. When compared to histograms of these quantities for the full mission period of 1995-2015 (see Figure 2

Table 1 Summary of MC fit parameter values for years 2004-2006.

Start					End		τ[a]	ϕ_A[b]	θ_A[b]	V[c]	$2R_0$[d]	B_0[e]	H[f]	χ_R[g]	asf[h]	CA[i]	Φ_0[j]	J_0[k]	Δt[l]	β_{CA}[m]	Ck[n]	I_0[o]	N[p]	$[\langle B_x\rangle\langle B_y\rangle\langle B_z\rangle]$[q]			f[r]	F[t]	Q_0[t]
Y-M-D	DOY	Hr	M	D	DOY	Hr	Hr	°	°	km/s	AU	nT			%	%	10^{20} Mx	μA km^{-2}	min	°	%	10^8 A		nT					
2004-04-04	095	2.8	04	05	096	14.8	36.0	76	69	434	0.393	22.6	L	0.093	2.6	−48	26.7	1.5	30	85	7.0	17.4	73	8.2	5.5	7.0	OK	OK	2
2004-07-22	204	15.4	07	22	204	23.1	7.8	67	−26	608	0.117	20.3	R	0.235	6.1	−18	2.1	4.4	15	70	−7.4	4.5	32	10.3	−0.3	−3.5	OK	OK	3
2004-07-24	206	12.8	07	25	207	13.3	24.5	86	−21	559	0.355	25.4	R	0.135	21.5	−30	26.5	1.8	30	87	−3.8	17.1	50	12.2	−4.1	−6.0	OK	OK	2
2004-08-29	242	18.7	08	30	243	20.8	26.0	54	−8	393	0.240	13.4	R	0.113	5.4	6	5.9	1.4	30	54	−16.8	6.1	53	9.0	−0.8	0.9	OK	OK	1
2004-11-08	313	3.4	11	08	313	16.6	13.3	47	−5	686	0.173	22.6	L	0.099	1.0	27	5.2	3.4	15	47	−1.7	7.7	54	12.0	−4.9	−6.3	OK	OK	2
2004-11-09	314	20.9	11	10	315	3.4	6.5	290	35	806	0.144	45.1	L	0.190	6.7	37	7.2	8.3	15	74	−7.9	13.0	27	23.1	0.9	−12.3	OK	OK	2
2004-11-10	315	3.6	11	10	315	11.1	7.5	37	−59	729	0.149	30.0	L	0.085	1.9	41	5.1	5.2	15	66	−10.8	8.7	31	15.8	−4.0	−10.8	OK	OK	2
2005-05-15	135	5.7	05	15	135	22.3	16.5	94	67	895	0.390	70.6	L	0.123	0.5	75	82.5	4.6	30	92	13.9	52.6	34	10.4	−5.9	−31.8	OK	OK	2
2005-05-20	140	7.3	05	21	141	5.3	22.0	221	59	456	0.179	17.9	L	0.161	13.1	−34	4.4	2.6	30	113	30.2	6.3	45	5.2	1.1	4.2	OK	OK	2
2005-06-12	163	15.6	06	13	164	7.1	15.5	128	−44	486	0.261	15.9	L	0.080	28.8	−28	8.3	1.6	15	116	−31.1	8.2	63	10.9	−1.8	5.1	OK	OK	2
2005-06-15	166	5.8	06	16	167	7.8	26.0	14	49	483	0.231	12.8	L	0.220	51.6	33	5.3	1.4	30	50	9.6	5.6	53	4.1	−2.1	−2.8	OK	OK	3
2005-07-17	198	15.3	07	18	199	3.8	12.5	79	−41	426	0.148	14.6	R	0.148	9.9	44	2.4	2.5	30	82	−3.1	4.1	26	5.9	3.6	4.6	OK	OK	2
2005-10-31	304	2.9	10	31	304	20.4	17.5	136	−16	372	0.106	12.9	R	0.235	2.1	−13	1.1	3.1	15	134	8.6	2.6	71	6.3	0.7	−1.4	OK	OK	3
2005-12-31	365	14.8	01	01	001	10.8	20.0	277	16	487	0.313	9.5	R	0.059	8.6	14	7.1	0.8	30	83	−27.1	5.9	41	6.9	−0.9	1.8	OK	OK	2
2006-02-05	036	19.1	02	06	037	13.1	18.0	106	−50	340	0.135	11.8	R	0.174	18.7	1	1.7	2.2	15	100	8.3	3.0	73	6.0	1.9	0.6	OK	OK	2
2006-04-13	103	14.8	04	13	103	20.8	6.0	244	77	528	0.096	20.5	L	0.085	40.7	0	1.5	5.5	10	96	−22.6	3.8	37	13.0	−4.3	−2.8	OK	OK	3
2006-04-13	103	20.6	04	14	104	9.9	13.3	262	−13	517	0.225	20.1	L	0.114	18.1	−23	7.8	2.3	15	98	−23.7	8.8	54	12.9	−3.3	5.3	OK	OK	2
2006-08-30	242	21.1	08	31	243	14.9	17.8	223	−8	411	0.134	10.9	L	0.135	2.6	−51	1.5	2.1	15	136	15.0	2.8	72	4.3	−1.2	4.1	OK	OK	2
2006-09-30	273	8.6	09	30	273	21.6	13.0	252	−16	392	0.097	21.8	L	0.133	25.8	−34	1.6	5.8	15	107	28.3	4.1	54	12.9	−3.3	5.3	OK	NOT	2

[a] τ: Duration (in Hr) of the MC encounter (i.e., τ = end time – start time of MC passage).

[b] φ_A, θ_A: Longitude and latitude (in ^{o}), respectively, of the MC axis (GSE coordinates).

[c] V: Average solar wind speed (in km s^{-1}) within the MC.

[d] $2R_0$: Estimated diameter (in AU), where R_0 is the model estimated radius.

[e] B_0: Estimated axial magnetic field magnitude (in nT).

[f] H: Handedness ($+1$ for right-handed or -1 for left-handed).

[g] χ_R: Square root of the reduced chi-squared of the MC fit

[h] asf (%): Asymmetry factor (in %) which depends on t_0 and τ; see Equation 9.

[i] $CA\ (\%) = Y_0/R_0$ (in %): Estimated relative closest approach distance where the estimated closest approach is Y_0, which is measured in the magnetic cloud (Cl) coordinate system.

[j] Φ_0: Estimated axial magnetic flux (in 10^{20} Mx); see Equation 11.

[k] J_0: Estimated axial current density (in μA km^{-2}); see Equation 10.

[l] Δt: Length (in min) of the averages used in the analysis; these are usually 15 min, 30 min, or 1 hour.

[m] β_{CA}: Cone angle, the angle between the MC axis and the X-axis (in GSE coordinates); see Equation 14.

[n] Check (ck): A check of the estimated radius by using duration, speed, CA and cone angle; see Equation 15.

[o] I_T: Estimated total axial current (in 10^8 A). See Equation 12.

[p] N: Number of points used in the MC fitting interval.

[q] $\langle B_{x,y,z} \rangle$: Average of the x, y, z component (in nT and cloud coordinates) over duration of the MC.

[r] The flag (f) to denote the ability to determine handedness (H), as OK or NOT.

[s] The flag (F) to denote the ability to determine convergence, as OK or NOT.

[t] Q_0: Estimated quality of the model fitting (where $Q_0 = 1, 2$, or 3, for excellent, good/fair, or poor, respectively) The criteria for quality (Q_0) are given in Appendix A of Lepping et al. (2006).

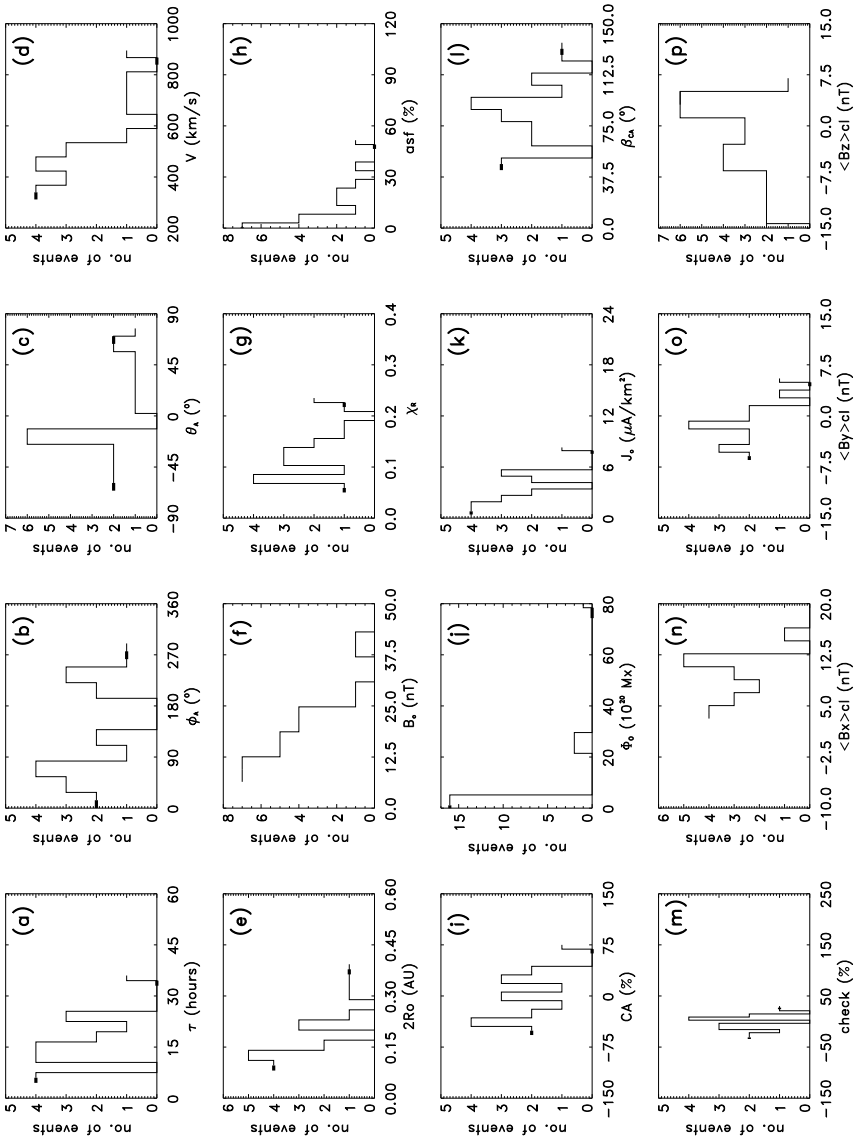

Figure 1 Histograms of Wind MC summary parameters for years 2004-2006, the Present period.

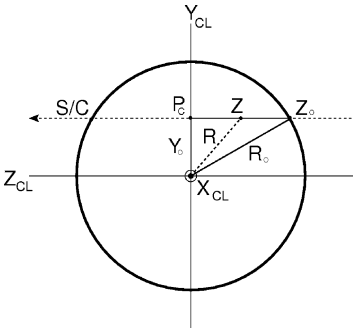

Figure 2 Representation of the MC cross-section in MC (Cl) coordinates; see Appendix B. The projection of the spacecraft path onto the cross-section defines the $\mathbf{Z}_{\mathrm{Cl}}$-axis in the Cl system, and Y_0 is the closest approach distance. Note that $\mathbf{Y}_{\mathrm{Cl}} = \mathbf{Z}_{\mathrm{Cl}} \times \mathbf{X}_{\mathrm{Cl}}$ in the Cl system, where $\mathbf{X}_{\mathrm{Cl}}$ is aligned with the axis of the MC (positive in the direction of the axial magnetic field), and Y_0 is along $\mathbf{Y}_{\mathrm{Cl}}$.

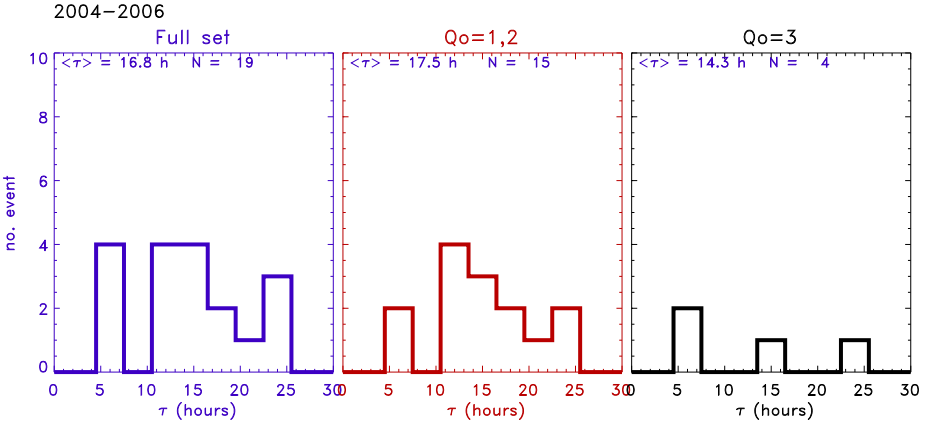

Figure 3 Histograms of the durations, i.e. the time that the spacecraft spends inside the MC, for the period 2004-2006, in terms of the full set ($Q_0 = 1, 2, 3$, on the left), $Q_0 = 1, 2$ (in the middle), and $Q_0 = 3$ only (on the right).

of Lepping et al., 2018a), the histograms in Figure 1 are similar to those of the long-term mission, except they are somewhat more irregular, as expected because they are based on a much smaller number of events (19 for the Present period versus 217 for the long-term set). Any other variations from one 3-year set of parameters to the next is probably due to the specific orientations and characteristics associated with the particular epoch of the solar cycle in which they occur.

Figure 3 shows histograms of the duration (τ), i.e. the time that the spacecraft spends inside the MC, for the Present period, 2004-2006, in terms of the full set (i.e. for $Q_0 = 1, 2, 3$), for $Q_0 = 1, 2$, and $Q_0 = 3$ only, as labeled at the top of the figure. Since there is a rather small number of events in the Present period ($N = 19$) (as in the next 3-year period with $N = 18$), we see a lack of smoothness in the histograms. Figure 4b of Lepping et al. (2018a), which shows durations in the same format as Figure 3 but for the Long-term period, 1995-2015 for comparison, gives a much better overall perception of this parameter, lacking any of the jaggedness in the histograms for the present set. The three τ-distributions for the Present period at least show values that lie within the bounds indicated by the Long-term period.

Table 2 presents the evaluated uncertainties on selected MC parameter values for qualities $Q_0 = 1$ and 2 only (quality is shown in the last column of the table) from Table 1, using the techniques described by Lepping, Berdichevsky, and Ferguson (2003, 2004). The

Table 2 Estimated uncertainties on MC parameter[a] values for sets $Q_0 = 1$ and 2.

Start date Year M D	σB_0 [nT]	σR_0 [0.01 AU]	σ asf [%]	$\sigma_{CA}(Y_0/R_0)$ [%]	$\sigma\theta_A$ [deg]	$\sigma\beta$[b](cone) [deg]	$\sigma\lvert\theta_A\rvert$ [deg]	Q_0
2004-07-24	2.1	1.0	17.1	30	13	25	11	2
2004-08-29	1.5	1.0	15.1	21	12	20	10	1
2004-11-08	2.4	1.0	15.3	21	12	20	9	2
2004-11-09	8.7	1.7	17.9	47	17	35	14	2
2004-11-10	2.0	0.8	14.5	20	10	19	8	2
2005-05-15	5.6	1.2	19.4	36	15	30	12	2
2005-05-20	3.0	1.5	18.1	38	16	30	13	2
2005-06-12	1.0	0.7	13.3	17	10	16	8	2
2005-07-17	1.6	1.3	18.3	37	15	30	12	2
2005-12-31	0.3	0.4	9.8	11	7	11	5	2
2006-02-05	1.4	1.2	16.9	31	14	26	12	2
2006-04-13	1.4	0.9	15.6	24	12	21	9	2
2006-08-30	2.1	1.5	18.5	35	16	29	12	2
2006-09-30	2.5	1.2	17.4	31	14	26	11	2

[a]Handedness (H) is not included. H is correct, unless the f-flag gives a NOT OK, as seen in Table 1.

[b]The error cone angle (β(cone)) represents the statistically estimated angle between the exact MC axis and the estimated axis, as defined by Lepping, Berdichevsky, and Ferguson (2003, 2004).

handedness parameter (H) is not included; see the footnote "a" of Table 2 which explains this. Table 3 shows the vector closest approach for all MCs of Table 1. In particular, Table 3 shows the MC start time, CA ($\equiv Y_0/R_0$ in %), $\boldsymbol{CA}$ (unit) (as a unit vector in GSE coordinates, with components yy and zz), $\boldsymbol{CA}$ (GSE) (as a vector in GSE coordinates in units of AU with components Y and Z), quality (Q_0), and S (state index defined by Equation 20); the x-component is zero, because the MC is assumed to be traveling along the x-axis in GSE locally, to a good approximation. See the Wind/MFI website

https://wind.gsfc.nasa.gov/mfi/mag_cloud_CA1.html

for further discussion of the concept of vector closest approach.

Table 4 presents mean values of the MC fit parameters and other quantities for the Present period, 2004 through 2006 (inclusive), and for other periods (discussed below). We give the number of events with $Q_0 = 1, 2, 3$, i.e. the total number; the number with only $Q_0 = 1, 2$, and percentage of total; duration the average values of the fundamental MC fit parameters (B_0, R_0, ϕ_A, θ_A, Y_0, H, t_0 (given in terms of asf); V, MC speed; the cone angle, β_{CA} (Equation 14); and so called derived quantities (J_0, I_T, and Φ_0 – Equations 10, 12, and 11), respectively); as well as other related parameter values associated with the fitting process, such as $\sqrt{\chi_{R^2}}$ reduced χ-squared), asf (%) (Equation 9), and Check (%) (Equation 15). Table 4 also includes two interplanetary (IP) parameters, average IP speed (IP V) and the interplanetary magnetic field (IMF), both for the same particular 3- year period, for comparison to those associated with the MC parameters of MC speed and B_0.

3. Statistically Modified Field Intensity Within MCs

Recently a scheme was developed by Lepping et al. (2018b) to provide a more realistic B/B_0 profile of a MC, than that used in the LJB model, based on the MCs studied earlier from the

Table 3 Vector closest approach with Q_0 and S (State index).

Start time[a]					$[Y_0/R_0]$[b]	$\boldsymbol{CA}$ (unit)[c]		$\boldsymbol{CA}$ (GSE)[d]		Q_0[e]	S[f]
Year	Month	Day	DOY	Hour	[%]	yy	zz	Y [AU]	Z [AU]		
2004	04	04	095	2.8	−48	0.94	−0.35	0.088	−0.033	2	−4
2004	07	22	204	15.4	−18	−0.47	−0.88	−0.005	−0.009	3	5
2004	07	24	206	12.8	−30	−0.36	−0.93	−0.019	−0.050	2	5
2004	08	29	242	18.7	6	0.17	0.99	0.001	0.007	1	1
2004	11	08	313	3.4	27	0.12	0.99	0.003	0.023	2	−11
2004	11	09	314	20.9	37	−0.60	−0.80	−0.016	−0.021	2	−2
2004	11	10	315	3.6	41	0.94	0.34	0.029	0.010	2	−14
2005	05	15	135	5.7	75	−0.92	0.39	−0.135	0.057	2	−3
2005	05	20	140	7.3	−34	0.93	0.37	0.028	0.011	2	−3
2005	06	12	163	15.6	−28	−0.77	−0.63	−0.028	−0.023	2	−14
2005	06	15	166	5.8	33	−0.98	0.21	−0.037	0.008	3	−15
2005	07	17	198	15.3	44	−0.28	0.75	−0.022	0.024	2	1
2005	10	31	304	2.9	−13	−0.38	−0.92	−0.003	−0.006	3	1
2005	12	31	365	14.8	14	−0.28	−0.96	−0.006	−0.021	2	15
2006	02	05	036	19.1	1	0.78	0.63	0.001	0.000	2	5
2006	04	13	103	14.8	0	NA	NA	NA	NA	3	−4
2006	04	13	103	20.6	−23	−0.23	0.97	−0.006	0.025	2	−1
2006	08	30	242	21.1	−51	−0.20	0.98	−0.007	0.033	2	−1
2006	09	30	273	8.6	−34	−0.29	0.96	−0.005	0.016	2	−1

[a]Start time in Year, Month, Day of Month, DOY (day of year), Hour, as labeled in the table.

[b]$CA \equiv Y_0/R_0$ (in %) (a scalar quantity); this is along the Y-axis in cloud coordinates.

[c]$\boldsymbol{CA}$ (unit) is $\boldsymbol{Y}_0/|Y_0|$, as unit vector (yy, zz), in GSE coordinates, where the X-component (xx) is zero.

[d]$\boldsymbol{CAu}$ (GSE) is $\boldsymbol{Y_0}$ (Y, Z) expressed in GSE coordinates in units of AU.

[e]Quality, Q_0.

[f]State is defined by Equation 20 (S = category × H, where H is handedness and category is defined in Table 5).

Wind spacecraft (see also Lepping, Berdichevsky, and Wu (2017) who provide the initial ideas on the formulation of the scheme). To briefly review how the scheme was developed, we examined the first 21 years of Wind magnetic field intensity in MCs, in terms of both the actual observations and as derived from the LJB model, the purpose being to obtain the difference-field intensity (i.e. observations – LJB Model) called Diff for each MC and then to obtain averages of these over the many MCs available at that time, but restricted to Q_0 of only 1 and 2 (see Appendix C). This restriction was applied in order to make more likely that acceptable quality would result; this provided 124 MCs. However, this was done with proper normalizations, i.e. B was normalized by B_0 (so strong fields could be properly averaged with weak ones) and "time" was essentially replaced by the percent of spacecraft passage through the MC (so large MCs could be averaged with small ones) before any averaging; the values of B_0, the magnetic field intensity on the MC axis, were estimated from the LJB model in each case.

By examining such difference fields we observed that they would vary according to the value of closest approach (CA) of the spacecraft to each of the MC's axes, the impact param-

eter, but apparently they would not be a strong function of CA (later, this was shown to be true.) Hence, we arbitrarily chose to split the analysis up into a "family of results" according to the CA estimate (with *CA*: 0-25, >25-50, >50-75, and >75-100), four sectors appear to be sufficient, remember $CA \equiv Y_0/R_0$ in %. Therefore, we could then produce four curves of Diff versus %-duration after averaging over 124 events, one curve for each of the four CA ranges. These curves were fitted with both quadratic and cubic curves (essentially to smooth each), and it was shown that the cubic curves provided little advantage over the quadratic curves in terms of their sigmas. So the quadratic curves were accepted as good representations of the average difference intensities and were referred to as the Quad formulae. That is, we have a set of four equations (parameterized according to CA) that represent the average difference field intensities (from the 124 MCs) between the observed MCs and the LJB model values, i.e. $Quad(CA, u) =$ Average of $\{B/B_0 -$ LJB model intensity$\}$, and where u is the distance measured along the spacecraft path through the MC in percent duration. This can be written as

$$Quad(CA, u) = \langle B/B_0 \rangle - \text{LJB model intensity}, \tag{1}$$

since LJB model intensity $= \langle$LJB model intensity$\rangle$. Finally, it is assumed that the Quad formulae (for the proper CA values), even though derived from averages of many MCs, will render more accurate the B profiles of future individual MCs when correctly applied as modifications, for any Q_0. See Lepping, Berdichevsky, and Wu (2017) and Lepping et al. (2018b) for more details on the foundation of the scheme.

Based on Equation 1, we then make the assumption that

$$\langle B/B_0 \rangle \Rightarrow B(\text{est})/B_0 \approx [\text{LJB model} + Quad(CA, u)], \tag{2}$$

for any individual event, where $B \Rightarrow B$(est) is the new *estimation* of B, so called because of the addition of the Quad modification term to the LJB model field, and again u is the distance measured of the spacecraft path through the MC in percent duration for the four possible relative closest approach sectors mentioned above (*CA*: 0-25, >25-50, >50-75, and >75-100).

The ratio $\Delta\sigma_N/\sigma_{N2}$ as described by Lepping et al. (2018b) was shown to be a good measure of how well the Quad scheme is performing, where the quantities σ_{N2} and $\Delta\sigma_N$ are defined here:

First we define

$$\text{Diff}_N \equiv (\text{Obs} - \text{Model}), \tag{3}$$

which is also a function of u, Obs are the actual field observations, and Model refers to the LJB model values, which we recall will depend on the value of *CA*. We define σ_N (where subscript N is for the 'new" Quad equations, as described by Lepping et al., 2018b), to be used in objective testing when comparing the B profiles, as

$$\sigma_{N1} \equiv \sigma_N\{\text{Obs} - \text{Model}\} = \left[(1/101)\sum(\text{Obs(U)} - \text{Model(U)})^2\right]^{1/2} \tag{4}$$

where $\sigma_N\{\}$ is an operator representing the root-mean-square of the quantities enclosed, $\sum$ sums over 101 points (i.e. including the two end points), and

$$\sigma_{N2} \equiv \sigma_N\{\text{Diff}_N - \text{Quad}\} = \left[(1/101)\sum(\text{Diff}_N\text{(U)} - \text{Quad(U)})^2\right]^{1/2}. \tag{5}$$

We define $\Delta\sigma_N$ as

$$\Delta\sigma_N = \sigma_{N1} - \sigma_{N2} \equiv \sigma_N\{\text{Obs} - \text{Model}\} - \sigma_N\{\text{Diff}_N - \text{Quad}\}. \quad (6)$$

The ratio $\Delta\sigma_N/\sigma_{N2}$ is a measure of the improvement in the B/B_0 fit to the MC B profile by using the Quad formulae as in Equation 2 (measured by $\Delta\sigma_N$) but weighted by the "accuracy" of the final fit (as measured by σ_{N2} in the denominator), since σ_{N2} is a quantitative measure of how well the Quad equations fit the Diff_N-profile (i.e. the difference between the actual observations and the LJB model values). The ratio of $\Delta\sigma_N/\sigma_{N2}$ may also be understood by realizing that it equals $(\sigma_{N1}/\sigma_{N2} - 1)$, and for good cases we always expect $\sigma_{N1} > \sigma_{N2}$, so that $(\sigma_{N1}/\sigma_{N2} - 1)$ is positive for good cases, as expected. We now make the subjective suggestion that when $\Delta\sigma_N/\sigma_{N2}$ is above 0.5 the scheme is doing very well (or it is exceptional), and when this ratio is between 0.0 and 0.5 the scheme is acceptable. However, when this ratio is negative the scheme is a failure, and this is an objective evaluation. It was shown statistically that this Quad scheme should improve MC profiles approximately 82% of the time (Lepping et al., 2018b).

Figure 4 shows plots of B/B_0 versus time for all 19 MCs studied here, in terms of actual observations (101 averages across each MC, shown by the black-continuous and non-smooth curve, called the Obs curve), the original Bessel function model profile (the black-continuous and smooth curve, described in Appendix A) and the new statistically modified version (the red dashed curve). Within each panel of Figure 4 (at the top) is the date, relative closest approach percentage ($CA \equiv Y_0/R_0$ in %), quality of the fit (Q_0), and average plasma speed within the MC ($\langle V_{MC} \rangle$). Below each set of curves is the value for the ratio $\Delta\sigma_N/\sigma_{N2}$, to help in evaluating the merit of the scheme for each case. As we see in Figure 4, most cases show successful usage of the Quad technique, i.e. positive values of $\Delta\sigma_N/\sigma_{N2}$ (16 cases, or 84% of the total). So most of the MCs in Figure 4 show a successful application of the Quad B/B_0-modification scheme described by Lepping et al. (2018b); only three cases (panels A, I, and O) should be considered failures, where $\Delta\sigma_N$ is negative, i.e. 16% of the total. Notice that in case O $\Delta\sigma_N$ is close to 0.00, so it just barely failed, and nine cases (panels B, C, F, G, J, N, P, Q, and S), where $\Delta\sigma_N/\sigma_{N2}$ is > 0.5, are exceptionally good, i.e. 47% of the total.

Now we present some detailed comments on the panels of Figure 4. First, the smaller the CA value the higher the peak B/B_0 of the Bessel functions (solid black curve). For example, panel Q has a $CA = 0\%$ and a maximum peak of $B/B_0 = 1.0$; similarly notice that panels D and O with small, but non-zero CAs, have B/B_0 values less than but near 1.0. By contrast panel H with a rather large $CA = 75\%$ (largest of all panels) has the lowest peak value of all panels. Second, all Bessel-function values start and end with the same B/B_0 value of 0.520; this is not surprising, since the axial component of the model vanishes at the boundary (and ideally the axial component of the observed field is always very close to vanishing). Third, the best performance of the Quad correction technique occurs for panels, F (with $\Delta\sigma_N/\sigma_{N2} = 1.612$), N (with $\Delta\sigma_N/\sigma_{N2}$ = 1.254), S (with $\Delta\sigma_N/\sigma_{N2}$= 1.252), B (with $\Delta\sigma_N/\sigma_{N2}$ = 1.115), i.e. all with $\Delta\sigma_N/\sigma_{N2}$ ratios greater than 1.1. There were six cases with $\Delta\sigma_N/\sigma_{N2}$ greater than 1.0, including the four listed above. For these four cases we see that the corrections (red dashed) curves reproduce the original data (Obs) very well, and extremely well in the case of panel F with the largest $\Delta\sigma_N/\sigma_{N2}$.

On the other hand, there were three cases (A, I, O) that had negative ($\Delta\sigma_N/\sigma_{N2}$) values, meaning that they were failures. When the corrected curve (red dashed) is (1) successful in its attempt to reproduce the Obs curve and (2) better than the Bessel-function (solid black) attempt to do the same thing, then we can expect the $\Delta\sigma_N/\sigma_{N2}$ values to be at least good/very good (i.e. usually in the range: $0.5 < \Delta\sigma_N/\sigma_{N2} < 1.0$, or sometimes with even

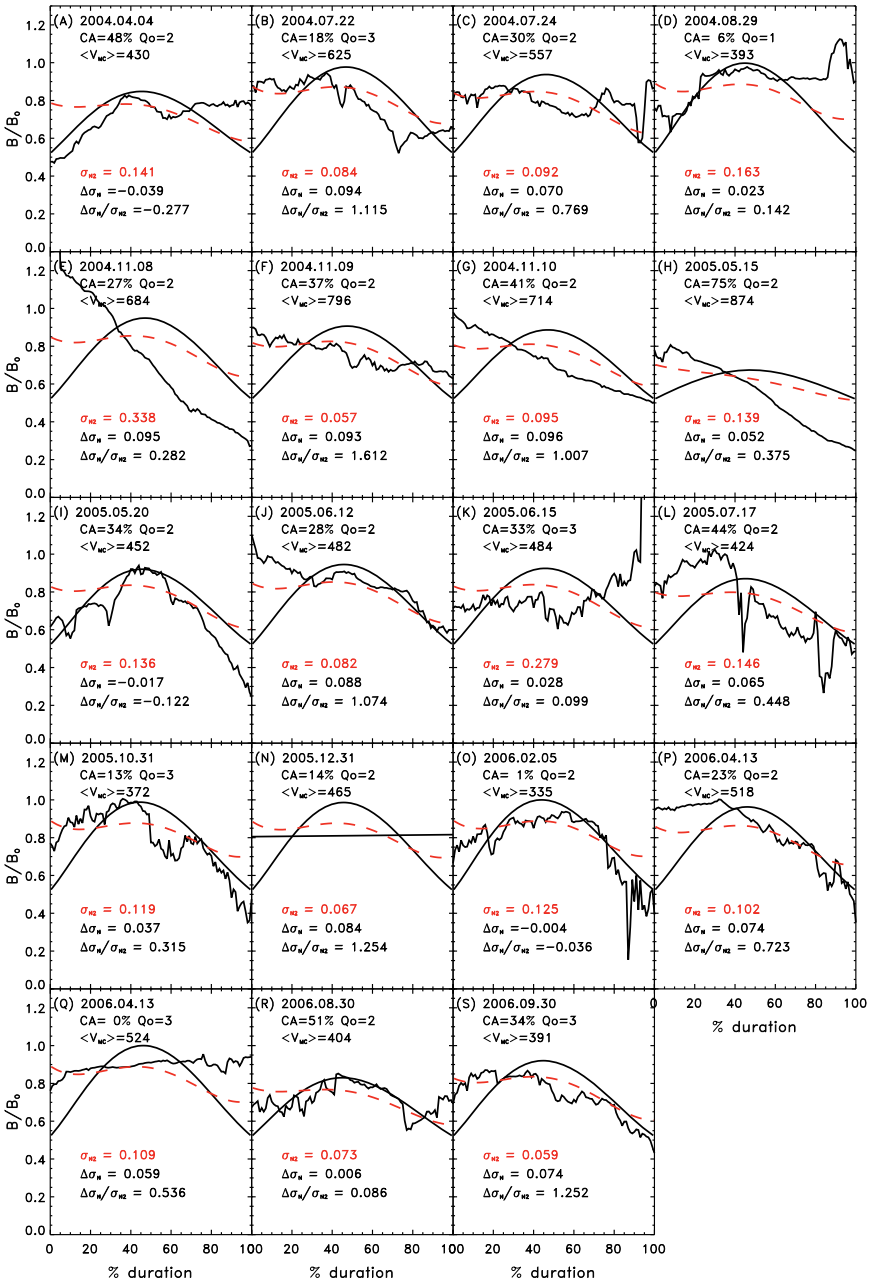

Figure 4 Plots of B/B_0 vs. time for all 19 MCs studied here, in terms of actual observations (101 averages across each MC, shown by the black-continuous and non-smooth curve, called the Obs curve), the original Bessel function model profile (the black-continuous and smooth curve, described in Appendix A), and the new statistically modified version of B/B_0 (the red dashed curve). At the top of each panel is the date of the event (in year, month, and day of month), the closest approach percentage ($CA \equiv Y_0/R_0$ in %), quality of the fit (Q_0), and average plasma speed within the MC ($\langle V_{\rm MC}\rangle$). Below the curves are values for the quantities $\sigma_{\rm N2}$, $\Delta\sigma_{\rm N}$, and $\Delta\sigma_{\rm N}/\sigma_{\rm N2}$, where the first two quantities are defined by Equations 5 and 6, respectively (and see Lepping et al., 2018b; Lepping, Berdichevsky, and Wu, 2017, which describe the B/B_0- modification scheme).

a higher upper limit). These are two separate considerations, measured by σ_{N2} and $\Delta\sigma_N$, respectively. Returning to panel F, we see that σ_{N2} has the smallest value of all of the panels, so it is an excellent success, and its $\Delta\sigma_N$ has one of the largest positive values of all panels. These are the reasons that panel F gives the best (largest) value of $\Delta\sigma_N/\sigma_{N2}$ (1.612). Notice that not only does the red curve match very well the Obs curve in panel F, but the red curve is distinctly better than the Bessel function curve for this MC. Notice that panel S generally has similar characteristics to panel F.

Now we point out an odd case, panel E: both the Bessel-function curve and the red curve are poor representations of the Obs curve, but the red curve is better, and therefore the Quad technique is successful ($\Delta\sigma_N = 0.095$). Hence, $\Delta\sigma_N/\sigma_{N2}$ ($= 0.282$) is positive, even if not very large, as expected.

4. Some Comparisons of Parameter Averages to Those of Earlier and Later Periods

Table 4 shows average values for the same quantities (MC fit parameters, derived quantities, etc.) as those presented for the Present period, 2004-2006 (see Section 2), but now for the periods 2007-2009, inclusive, 2010-2012, and 2013-2015 (as designated at the top of the table), as well as for the Long-term period, 1995-2015 (called Long-term, in the last column). First, we see that the number of MCs (N = 19) in the Present period was almost the same as that for the period 2007-2009, and then we see a marked increase of MCs for each of the next two 3-year periods. Note that the Long-term period has 217 MCs over 21 years, i.e. on average 31 MCs per each 3-year-period but, as noted, the last two 3-year periods have 48 and 49 MCs, respectively. The rate of MC occurrence for the four periods, 2004-2006, 2007-2009, 2010-2012, 2013-2015 is 6.3/year, 6.0/year, 16.0/year, 16.3/year, respectively, compared to a rate of 10.3/year for the Long-term period. Over the last decade shown, MC durations do not vary much, i.e. none are outside of about 20% of the value of the Long-term period of 19.2 hours.

We refer to Lepping et al. (2018a) for model-derived characteristics of Wind MCs for years 1995-2015, the Long-term period. We see that during the Present period the MCs are, on average, faster (by 21%), stronger in axial magnetic field, B_0 (by 37%), and smaller in diameter (by 6.5%), than those in the Long-term period. The quality of the MCs in the Present period is much greater than that of the Long-term period, where the ratio of $N(Q_0 = 1, 2)$ to $N(Q_0 = 1, 2, 3)$ is 0.79 (see 79% in the second line of Table 4) for the Present period and 0.58 for the Long-term period as pointed out above. The average speed of the MCs in the Present period (527 km s^{-1}) was distinctly higher than that of most of the other periods, and similarly $\langle B_0 \rangle$ (of 22.0 nT) was the highest of all periods. The quantities J_0, Φ_0, and I_T are all proportional to B_0 and are dominated by it when $\langle R_0 \rangle$ does not vary much from one set to another (as is the case here), as shown by Equations 10, 11, 12 of Appendix A. Hence, the relatively large value of $\langle B_0 \rangle$ for the Present period compared to those of the other periods yields quite large values for J_0, Φ_0, and I_T for the Present period, as seen in Table 4. It is interesting that asf is quite low compared to those of the other periods; this is not easy to interpret and may be only coincidental. Notice that $\sqrt{\chi_{R^2}}$ for the Present period was the smallest of those of all of the other sets; this is consistent, we believe, with the fact that the average quality of the MCs in the Present period is much greater than that of the Long-term period and of the other three periods. So generally the Present period is quite different from the Long-term period, as it is from the other three

Table 4 Comparison of the averages and σ's [in brackets] of the physical characteristics of MCs for the present, recent, and long-term sets for $Q_0 = 1, 2, 3$.

Quantity	2004-2006[a] Period	2007-2009[b] Period	2010-2012[c] Period	2013-2015[d] Period	1995-2015[e], Long-Term
$N(Q_0 = 1, 2, 3)$	19	18	48	49	217
$N(Q_0 = 1, 2)$	15 [79%]	10 [56%]	22 [46%]	27 [55%]	125 [58%]
Duration (hrs)	16.8 [7.8]	15.1 [7.8]	17.3 [9.8]	20.3 [10.5]	19.2 [10.1]
V_{MC} (km s^{-1})	527 [142]	359 [46]	415 [77]	425 [85]	436 [109]
IP V (km s^{-1})	452 {426}[i]	419	411	411	429 {406}[i]
IMF (nT)[f]	5.9 {5.2}[i]	4.2	5.2	6.0	5.9 {5.2}[i]
B_0 (nT)	22.0 [14.4]	11.0 [4.2]	13.6 [5.9]	14.7 [5.7]	16.1 [7.8]
R_0 (AU)	0.205 [0.101]	0.169 [0.086]	0.173 [0.086]	0.231 [0.128]	0.217 [0.115]
$\lvert Y_0\rvert/R_0$ (%)	29 [19]	36 [28]	31 [28]	38 [28]	38 [29]
Handedness[g]	7 R and 12 L	11 R and 7 L	24 R and 24 L	22 R and 27 L	101 R and 116 L
$\lvert\theta_A\rvert$ (degrees)	36 [23]	32 [20]	36 [23]	39 [21]	35 [22]
ϕ_A (degrees)[h]	75 [11]	91 [15]	105 [8]	103 [9]	96 [4]
β_{CA} (degrees)	89 [26]	86 [27]	89 [33]	85 [27]	90 [30]
J_0 (μA/km^2)	3.2 [2.0]	2.0 [1.1]	2.8 [2.4]	2.2 [1.7]	2.6 [2.4]
I_T (10^8 A)	9.6 [11.5]	3.6 [2.0]	4.5 [2.8]	6.3 [3.5]	8.1 [6.5]
Φ_0 (10^{20} Mx)	10.7 [19.0]	2.9 [2.6]	3.8 [3.9]	7.0 [7.5]	7.7 [10.8]
$\sqrt{\chi_{R^2}}$	0.138 [0.055]	0.144 [0.055]	0.173 [0.079]	0.165 [0.077]	0.153 [0.066]
asf (%)	14.0 [14.7]	29.8 [30.9]	29.3 [36.1]	30.3 [49.6]	25.5 [35.6]
|checkl (%)	14.6 [9.7]	25.6 [23.2]	18.4 [22.8]	17.4 [13.8]	22.6 [37.8]

[a]The Present Period is defined as the period 2004-2006, inclusive.

[b]For MC fitting results of the years 2007 to 2009, inclusive, see Lepping et al. (2011).

[c]For MC fitting results of the years 2010 to 2012, inclusive, see Lepping et al. (2015).

[d]For MC fitting results of the years 2013 to 2015, inclusive, see Lepping et al. (2018a).

[e]The Long-term Period is defined as years 1995 to 2015, inclusive, and includes the results of this study.

[f]IMF(nT) refers to an average external interplanetary magnetic field for the period designated.

[g]MC Handedness is R for right-handed (H = +1) and L for left-handed (H = −1).

[h]If ϕ_A is greater than 180°, then 180° is subtracted from ϕ_A before the average over the set is taken.

[i]The value in the { } symbols refers to the median value, for IP V or IMF.

3-year periods between 2007 and the end of 2015, and in most respects it is superior (except for having a smaller number of events than most of the others); see Lepping et al. (2011, 2015, and 2018a) for analyses and descriptions of these other periods, in time order.

5. Magnetic Cloud Type

Table 5 provides the definitions of MC Type in terms of ten categories, and associated code numbers are also given for convenience. An alternative designation of MC Type is given by Mulligan, Russell, and Luhmann (1998) (also see Bothmer and Rust, 1997) wherein they

Table 5 Definitions of magnetic cloud type categories[a].

Type	Definition[b]	Color[c]	Type	Definition[b]	Color[c]
1	N ⇒ S	black	11	S ⇒ N	dark green
2	N ⇒ S, mostly N	light green	12	S ⇒ N, mostly S	red
3	Almost all N	blue	13	Almost all S	orange
4	All N	dark blue	14	All S	magenta
5	N ⇒ S, mostly S	yellow	15	S ⇒ N, mostly N	purple

[a]These categories are qualitatively determined by visual inspection.

[b]N refers to northward magnetic field and S refers to southward, determined by the latitude (θ_B) of the magnetic field within the MC, in GSE coordinates, observed as the spacecraft passes through the MC. It is understood that N ⇒ S, for example, refers to a relatively smooth change from N to S, and likewise for S ⇒ N, etc.

[c]Color refers to the color of the bars in the histograms of Figure 5.

use three letters to represent the profile of the θ_B-variation within the MC; their "type" in a sense is equivalent to our "state" where we combine Type (defined by two letters in our case) with handedness, which in essence is their third letter (see Lepping et al., 2015).

In Figure 5 of Lepping et al. (2015) we show how the MC Type evolves over the period 1995 to 2012, in 3.5-year segments (on average). For example, the most striking change is the fact that category 1 (N ⇒ S, black) increases as it steps through the segments in time, i.e. it goes from 8% (for the first segment of 1995-1998, inclusive), to 21%, to 26%, to 78%, then down again to 27% (by the 2010-2012 segment). Whereas, by contrast, category 11 (S ⇒ N, green) goes from 33%, to 36%, to 21%, to 6%, and finally back to 15% over those same segments, i.e. for the most part, it decreases. So the most common categories 1 and 11 are somewhat inverse to each other in occurrence rate versus time. All other categories show much greater variability in this regard. Panel "Total," in Figure 5 of Lepping et al. (2015) covering 168 MCs (for the years 1995 to and including year 2012), shows very good symmetry when ordered in the following way, by code number (see Table 5): 1, 4, 3, 5, 2, 12, 15, 13, 14, 11. Panel a of Figure 6 of Lepping et al. (2018a) covers the more recent MC fittings of 2013-2015 MCs. So that when an even greater total number of MCs, by 49 events, is included in the "Total" histogram (shown in panel b of Figure 6, N = 217 and given here as Figure 5b, for convenience), we see that relatively good symmetry remains, with very low contributions (4% or less) from the four central categories of 2, 12, 15, and 13, where the category ordering is the same as that shown in panel "Total" of Figure 5 of Lepping et al. (2015). The infrequently occurring categories of 2, 15, and 13 of Figure 6b of Lepping et al. (2018a) are N ⇒ S, mostly N; S ⇒ N, mostly N; and Almost all S, respectively, as might be expected, since they represent the highly tilted cases. Such cases may be related in the solar cycle to the highly tilted solar magnetic dipole. Finally, we point out that, from Figure 5b (Long-Term period) this study, categories 3, 5, 2, 12, 15, and 13 have occurrences at 6% or lower, with category 15 as low as 2%. Now we consider the distribution of Types for the Present period in contrast to what we described above for the much larger set of MCs.

Figure 5a corresponds to the relatively small number N = 19 of MCs found in the present preriod; we arrange the bars along the horizontal axis following the pattern shown in panel b of Figure 5. First, in examining Figure 5a we again see that category 1 (black) is prevalent with a 32% occurrence rate (i.e. 6 events out of 19 total); it was 25% for the Long-term

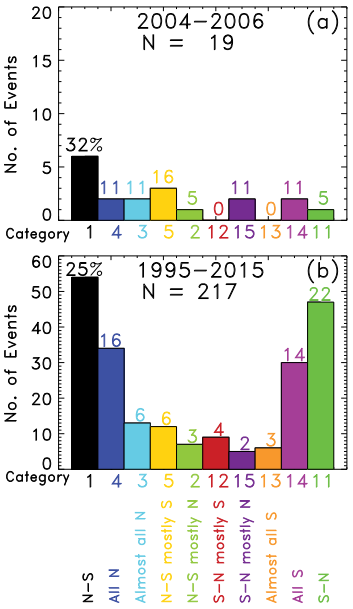

Figure 5 Histogram of Wind MC Type; see Table 5 for definitions of MC Type. (**a**) For the Present period (2004-2006) and (**b**) For the Long-term period (1995-2015); see Lepping et al. (2018a). Notice that the vertical scales differ by a factor of three between panels (a) and (b).

period of N= 217 (Figure 5b). Also, in panel a category 5 (yellow, N ⇒ S, mostly S) is somewhat prevalent, so that when the Types in category 1 and 5 are combined we get almost 1/2 (48%) of all of the MCs in the period 2004-2006. Notice that of the four infrequently occurring categories shown in Figure 5a (i.e. 2, 12, 13, 11), three of them usually contain highly tilted MCs (i.e. except category 11, see below); these are also infrequent in the long-term set, as we pointed out above for those types, with occurrences of 4% or less (i.e. except for category 11). However, we should not expect a completely fair comparison in this respect, since the statistics are poor with N = 19 MCs in the Present period. Category 11 (dark green), with a low occurrence rate of only 5%, as shown in Figure 5a, is much lower than that seen for the comparable bar in Figure 5b (the long-term value). The 5% is not inconsistent with what was seen in the past for this part of the solar cycle (where category 1 (black) is most prevalent), i.e. we should expect a low occurrence of category 11 at that phase, as in panel d of Figure 5 of Lepping et al. (2015) for the nearby years 2007-2009, where this asymmetry is even more exaggerated (78% for category 1, and 6% for category 11). A possible explanation for this is the changing tilt of the solar current sheet which varies with solar cycle and is expected to play an important role in influencing the inclination of MCs, as we pointed out in Lepping et al. (2018a). So there is nothing that is obviously irregular in this present set with regard to Type when compared to the long-term set, when solar phase is accounted for, even though we are dealing with rather poor statistics with only 19 events in the present set.

6. Related Upstream Shock Waves

In Table 6 we list the starting dates of the 19 MCs that were listed in Table 1, the present set. In column two of Table 6 there is an indication of whether the specific MC has an upstream shock wave (S) or no shock wave (no S). The specific values of the average magnetosheath speed ($\langle V_{\rm sheath}\rangle$), when applicable, and the 2-hour-average speed at

Table 6 MC events with upstream shocks and MC type designation.

Year-month-day	Shock = S No Shock = no S	{Type[a]}	$\langle V_{\rm sheath}\rangle$[b] (km s^{-1})	$\langle V_{\rm Front}\rangle$ (km s^{-1})	ΔV[c] (km s^{-1})
2004-04-04	S	{4}	502	518	−16
2004-07-22	S	{5}	473	523	−50
2004-07-24	S	{5}	590	575	15
2004-08-29	S	{1}	423	413	10
2004-11-08	S	{11}	661	694	−33
2004-11-09	S	{2}	729	816	−87
2004-11-10	S	{14}	803	764	39
2005-05-15	S	{3}	841	971	−130
2005-05-20	S	{3}	477	472	5
2005-06-12	S	{14}	432	502	−70
2005-06-15	S	{15}	526	507	19
2005-07-17	S	{1}	471	449	22
2005-10-31	no S	{1}	N/A (366)[e]	395	N/A [-29][f]
2005-12-31	no S	{15}	N/A (541)	495	N/A [46]
2006-02-05	no S	{5}	N/A (363)	354	N/A [9]
2006-04-13[d]	no S ?	{4}	N/A (435)	545	N/A [-110]
2006-04-13[d]	no S	{1}	N/A (497)	522	N/A [-25]
2006-08-30	no S	{1}	N/A (479)	440	N/A [39]
2006-09-30	no S	{1}	N/A (332)	433	N/A [-101]

[a]Type is MC type, in { } – see Table 5.

[b]The average of the sheath speed, or if there is no shock, we state N/A and put the V in ().

[c] $\Delta V = \langle V_{\rm sheath}\rangle - \langle V_{\rm Front}\rangle$. If there is no a shock, we state N/A and put the ΔV in brackets.

[d]Two MCs seen on 2006-04-13, and apparently neither had an upstream shock wave; see text.

[e]The value in parenthesis (called $V_{\rm IP}$) is the average speed over 12 hours immediately upstream of the MC for cases where no upstream (MC-driven) shock wave exists.

[f]For cases where there is no upstream shock, then $\Delta V_{\rm IP} = \langle V_{\rm IP}\rangle - \langle V_{\rm Front}\rangle$ replaces ΔV(shown in brackets).

the front of the MC ($\langle V_{\rm Front}\rangle$) are provided in columns 4 and 5, respectively. Note that the sheath is the region between the upstream shock and the front boundary of the MC when a shock exists, and we set a rule that the sheath interval must be less than 20 hours. The choice of 20 hours is somewhat strict, but is justified by Lepping et al. (2018a); we point out that the average duration for such upstream shock-MC sheaths from *Wind* data is estimated to be 12.1 hours (Wu and Lepping, 2016), and 2 × 12.1 hours easily covers 20 hours.

Table 6 shows the difference speed ($\Delta V = \langle V_{\rm sheath}\rangle - \langle V_{\rm Front}\rangle$) in the last column; this is the difference between the average sheath speed and the speed at the front of the MC. The value of the average speed, $\langle V_{\rm MC}\rangle$, taken over the duration of each MC is given in Table 1. When there is no upstream shock, we state N/A in columns 4 and 6, and then $\langle V_{\rm sheath}\rangle$ is replaced by the IP speed over 12 hours just before the front of the MC, and in those cases $\Delta V_{\rm IP} = \langle V_{\rm IP}\rangle - \langle V_{\rm Front}\rangle$ replaces $\Delta V = \langle V_{\rm sheath}\rangle - \langle V_{\rm Front}\rangle$, as listed in the last column. We believe that there is usually a correlation between $V_{\rm front}$ (or $V_{\rm MC}$) and $\langle V_{\rm sheath}\rangle$ based on our years of experience examining Wind MCs, with many having upstream driven shocks.

However, there have been studies where arguments have been made against a necessary cause-effect relationship between a given shock wave followed, in 20 or fewer hours, by the front of a MC/MCL structure (see, e.g., Berdichevsky et al., 1998 and 2005); these arguments are also based on the relative speeds of the shocks and their respective ejecta. But such cases are not very common.

There were 12 MCs with upstream shocks out of the 19 total cases (i.e. 63% of the total) in the present set, as shown in Table 6. Typically around 56% of MCs have upstream shock waves at 1 AU for the long-term average (e.g. Lepping et al., 2002, 2015; Wu and Lepping, 2016; Wu et al., 2017). So the percentage of cases with shock waves for this present set is only slightly larger than the long-term average. Since the present 3-year set is centered close to being mid-way point between the smoothed max and min sunspot numbers, i.e. at around years 2001 to 2009 (a declining phase), respectively, we should not be surprised at the approximate agreement between the present (63%) and the long-term (56%) percentages.

As Table 6 shows, for the upstream shock cases, the $\langle V_{\rm sheath}\rangle$ values may be smaller or larger than the $\langle V_{\rm front}\rangle$ values; in fact, six cases showed a positive value for $\Delta V = \langle V_{\rm sheath}\rangle - \langle V_{\rm front}\rangle$ and six showed a negative value. In Lepping et al. (2018a) the quantity $\langle V_{\rm sheath}\rangle - \langle V_{\rm MC}\rangle$ was determined for each MC that had an upstream shock for the period 2013-2015 (21 cases), and it was shown that this quantity was usually positive, but four cases were negative. The shift to more positive cases for the 2013-2015 set is understandable, since $\langle V_{\rm front}\rangle$ is almost always larger than $\langle V_{\rm MC}\rangle$, as most MCs are expanding. We chose to show $\Delta V = \langle V_{\rm sheath}\rangle - \langle V_{\rm front}\rangle$ for the present set, since the plasma just downstream of the sheath, is most closely characterized by $\langle V_{\rm front}\rangle$, not $\langle V_{\rm MC}\rangle$. See Lepping et al. (2002) for more statistics on the relative speeds of upstream shocks and the front boundaries of MCs at 1 AU from Wind data. In that study it was shown that, when such an upstream shock exists, $\langle V_{\rm MC}\rangle$ will usually be approximately equal to the speed of the shock. This indicates that the MC is very likely the driver of that shock.

We point out that in Table 6 there were two MCs listed for day 2006-04-13; see footnote d in the table. The front boundaries of these were at hours 14.8 and 20.6 of that day. We put a question mark in the second column of the table for the first of these cases, because there does occur an upstream discontinuity at 11:18 UT (or 11.295 hour) of that day that weakly suggests a shock ramp, but we believe that it is too uncertain to list as a definitive shock wave.

Finally, we call attention to the fact that all 12 upstream shocks listed in Table 6 occur in the early part of the 3-year present set, and therefore the seven no-Shock cases occur in the latter part with a separation between these two subsets occurring more or less in the early Fall of 2005. This separation is obviously correlated with the average MC speeds (and also with the front speeds of the MCs). For example, the average of $\langle V_{\rm MC}\rangle$ for the first 12 MCs is 580 km s^{-1}, whereas this average for the last seven MCs (i.e. the no-Shock cases) is 435 km s^{-1}. The first set is therefore 33% higher in speed than the second set, on average. If this same comparison is carried out using the front speeds of the MCs (instead of $\langle V_{\rm MC}\rangle$), we find the average of the first 12 cases is 600 km s^{-1} and that of the last seven is 455 km s^{-1}. Hence, the first set is 32% higher in speed than the second, similar to the 33% derived above. So we see that in both results there is a considerable difference in average speeds between these two subsets. This is at least partly due to the phase of the solar cycle (more on this in the Summary), but the fact of the sharp separation is somewhat surprising and not understood.

7. Summary and Discussion

- **The Study's Overall Purpose**

This work is a continuation of our overall study of Wind interplanetary MCs. The MC least-squares fitting results, using the model of Lepping, Jones, and Burlaga (1990), are based on Wind data during the Present period, defined as the three years 2004-2006. In terms of average parameter values we compare the model fitting results from the Present period to the results of the full mission, i.e. years 1995 to the end of 2015 (called the Long-term period here and which includes the Present period), and these are further compared to the results of three other recent studies that encompassed the periods 2007-2009 and 2010-2012, 2013-2015, inclusive (see Table 4). The present model fitting results are added to the Wind/MFI MC website, i.e. the parameter values shown in Table 1, and other related tables are provided; see the beginning of Section 2. MC Type and upstream driven shock waves are also discussed, as well as the results of our recent work on modifying the MC intensity profiles.

- **Highlights of MC Model Fitting Results for the Present Period and Comparisons to Other Periods**

For the first nine years of the Wind mission (i.e. up to and including year 2003) the occurrence rate of MCs was 9.2 events/year, similar to the long-term rate of 10.3/year. Just as for the period 2007-2009, the occurrence rate for the Present period was low at 6.3/year. The rate increased markedly over the years 2010-2015, to about 16/year. Also during the Present period the MCs were, on average, significantly faster (by 21%), much stronger in axial magnetic field (by 37%), and smaller in diameter (by 5.5%), than those in the Long-term period. The quality of the MCs in the Present period is significantly better than that of the Long-term period, i.e. the ratio of N($Q_0 = 1, 2$) to N($Q_0 = 1, 2, 3$) for the Present period is 0.79, whereas it is 0.58 for the Long- term period. An outstanding feature of the Present period is its high average B_0, which was 22.0 nT, i.e. twice that of the 2007-2009 period and even 37% higher than that of the Long-term period. That large average B_0 is mainly responsible for the unusually large average values of J_0, I_T, and Φ_0 in the Present period, which were 23%, 17%, and 39% higher, respectively, than those values of the Long-term period; see Equations 10, 12, and 11, respectively, for the estimating these quantities. (R_0 also plays an important role in estimating Φ_0, as Equation 11 shows.) Also we see that the average V_{MC} is distinctly higher (at 527 km s^{-1}) than those of the other periods shown in Table 4, including that for the Long-term period, which was 436 km s^{-1}, i.e. 21% higher. However, as V_{MC} very high σ-value of 142 km s^{-1} indicates (see Table 4), the main reason for the high average of 527 km s^{-1} is the large contribution of a few very high values of speeds (also see Table 1). A similar argument can be used concerning the large average of B_0. This feature is the main reason that the average duration is 12.5% lower than that of the Long-term period, which is 19.2 hours. In summary, the Present period has many characteristics that differ from those of the other 3-year periods shown in Table 4 including those of the Long-term period. It is unique.

- **Summary of Statistically Modifying MC Field Intensity Profiles**

Recently a scheme was developed by Lepping et al. (2018b) to provide a more realistic B/B_0 profile of a MC than that used in the LJB model, which is strictly based on the Bessel-function solution as described in Appendix A. The modification of the B/B_0 profile in this scheme is based on a study of the magnetic fields of MCs from the Wind spacecraft using over 21 years of data (Lepping, Berdichevsky, and Wu, 2017). It was shown statistically

by Lepping et al. (2018b) that this scheme, called the Quad technique, should improve MC profiles at about 82% of the time using a long-term set of MCs.

Figure 4 presents plots of B/B_0 versus time for all 19 MCs of the present set studied here in terms of actual observations, the original Bessel-function model profile (described in Appendix A), and the new statistically modified version of B/B_0 (the red dashed curve). Figure 4 shows successful usage of this technique, i.e. positive values of $\Delta\sigma_N/\sigma_{N2}$ in 84% of the total for the present set of MCs; the arguments that the use of the ratio $\Delta\sigma_N/\sigma_{N2}$ (whose specific values are shown in the panels of Figure 4) is proper for judging success or failure, and degree of success, of the technique is given by Lepping et al. (2018b). So most of the MCs in Figure 4 show a successful application of this B/B_0-modification scheme; only three cases should be considered failures, where $\Delta\sigma_N$ was negative, i.e. 16% of the total. In nine cases (i.e. panels B, C, F, G, J, N, P, Q, and S of Figure 4) the values are exceptionally good. This is almost 1/2 of the total. Hence, this set of 19 MCs (with respect to success or failure) gives results that are consistent with the much larger number (N = 124) of MCs used in developing the Quad technique (Lepping, Berdichevsky, and Wu, 2017).

We point out that when the field magnitude is modified in this manner in the MC parameter fitting model, we are abandoning the force-free assumption, but this assumption is probably not very seriously violated by this modification. However, a quantitative proof of this belief is beyond the scope of this work. We suggest that the field magnitude modification (the Quad addition) to the Bessel field is apparently due to all of those factors that could possibly contribute to a violation of the force free and/or circular cross-section assumptions. The most obvious contributors are: (1) Perturbations from force-free at the Sun, the birthplace of the MC ejection. (2) Interactions (especially compression), front and rear of the MC, with the ambient solar wind as it travels away from the Sun; this includes any evolution of the cross-sectional shape of the MC. (3) Expansion of the MC as it travels away from the Sun which occurs in the vast majority of cases. The proper sum (possibly a weighted sum) of these effects, if they are the only relevant ones, should ideally and fully make up the Quad modification, at least in an average way. Hence, the proper characterizations of items 2 and 3 above, i.e. MC interactions and expansion, respectively, should provide us with item 1 when they are subtracted from the Quad term, which in this rendition is considered a constraint in the problem of understanding the average MC birthplace conditions. Fortunately item 3 is relatively well understood. However, since only average considerations are expected from such an exercise, its results may be difficult to interpret.

- **Summary of MC Types**

Figure 5 shows the distribution of MC Types for (Figure 5a) the Present period (N = 19) and for comparison (Figure 5b) the Long-Term period (N = 217). In Figure 5a we see that categories 1 (black) and 5 (yellow) are most prevalent for years 2004-2006, and that when Types 1 and 5 are combined we get almost 1/2 of all of the MCs in the period (48%); in fact, category 1 alone has a 32% contribution. Generally speaking these two categories are of the N ⇒ S Type. The types under the general category of S ⇒ N occur on the right side of Figure 5a and at this part of the solar cycle they are relatively infrequent. Category 1 is also very common in the long-term set (at 25%), but category 11 (green) on a long-term basis is also common (at 22%), as Figure 5b shows; we recall that the long-term set covers 21 years, i.e. almost two solar cycles or one magnetic solar cycle. It should not be surprising that categories 1 (N ⇒ S) and 11 (S ⇒ N) are so common on a long-term basis, since observations of their profiles in effect were how MCs were recognized in the first place by L. Burlaga and coworkers almost 40 years ago (see Burlaga et al. (1981) and Burlaga (1995) for a review of the early observations of MCs).

We point out that the intermediate occurring types in Figure 5a at 11% each are all related in some way with strongly inclined MCs (categories 4, 3, 15, and 14, in order, i.e. All N, almost all N, S ⇒ N mostly S, and All S). It should be expected that there is a considerable contribution from these categories when combined (44%), since the changing tilt of the solar current sheet is generally expected to play a dominant role in influencing the inclination of MCs at this epoch. In summary, the Type distribution of the present set when compared to the long-term set and when solar phase is accounted for, has rather expected features, even though at N = 19 MCs we are confronted with rather poor statistics in the present set. Hence, this present set of MCs, as unique as it is in many respects (as pointed out elsewhere) is not so with regard to Type.

- **Summary of Upstream Shocks**

There were 12 MCs with upstream shock waves in the present set. This represents 63% of the full set of N = 19 MCs. Usually 56% of MCs have upstream shock waves at 1 AU based on long-term Wind data (e.g. Lepping et al., 2002; Lepping et al., 2015; Wu and Lepping, 2016; Wu et al., 2017). So the percentage of MCs with upstream shocks in the present set is comparable with long-term statistics, though somewhat higher for the present set. The fact that there is a relatively consistent rate of MCs with upstream shocks in this present interval compared with the long-term rate is consistent with the present set being about midway between solar maximum and solar minimum (a declining phase), occurring approximately in the years 2001 and 2009, respectively. Table 6 gives a list of all MCs for the present set and shows those that have upstream shocks, and it compares average magnetosheath speeds ($\langle V_{\rm sheath}\rangle$) with the speeds at the front of the MC ($\langle V_{\rm front}\rangle$) in the last column where $\Delta V = \langle V_{\rm sheath}\rangle - \langle V_{\rm front}\rangle$. When there is no upstream shock, then $\langle V_{\rm sheath}\rangle$ is replaced by the IP speed averaged over 12 hours just before the front of the MC, and in those cases $\Delta V_{\rm IP} = \langle V_{\rm IP}\rangle - \langle V_{\rm front}\rangle$ replaces ΔV in the last column. We see that actual average sheath speed in the present set, when there is an upstream shock wave, can be either larger or smaller than the $\langle V_{\rm front}\rangle$ values, almost in equal numbers (and the average of the negative ΔV set is larger in absolute value than the average of the positive ΔV set). We point out that shock waves are also seen to occur within MCs but only for a small percentage of observed cases; an example of this was pointed out by Collier, Lepping, and Berdichevsky (2005).

It turns out that there is an interesting, and somewhat dramatic, separation in average MC speed between the first 12 MCs (i.e. the average speed over only the MCs with upstream shock waves of the full set) and the last seven MCs (those without upstream shocks), whereby the earlier ones are 33% faster. The first 12 MCs have average speeds ranging from 413 km s^{-1} to 971 km s^{-1} and the last seven have average speeds ranging from 354 km s^{-1} to 545 km s^{-1}. If this separation is examined in terms of the speeds of the front of the MCs (i.e. using $\langle V_{\rm front}\rangle$, instead of using $\langle V_{\rm MC}\rangle$) we see that the first 12 are 32% faster than the last seven, very close to that determined by using $\langle V_{\rm MC}\rangle$. The separation between these fast and slow subsets occurs more or less in the early Fall of 2005. This is consistent with the variation of the sunspot number (SSN) in the following sense. Using a 13-month smoothed SSN (see http://www.sidc.be/silso/ssngraphics) we see that, in the temporal vicinity of our interest, there is a second peak at year 2001 and a minimum at year 2009. The mid-point of these is therefore in the year 2005, consistent with our speed separation.

It has been noticed that MCs that possess an upstream shock tend to cause more intense geomagnetic storms than MCs without such a shock, as discussed by Wu and Lepping (2015, 2016). Hence, we believe that the subject of MC-driven shock waves takes on even greater importance than it would otherwise.

Acknowledgements We thank the Wind/MFI and SWE teams for the care they employ in producing the magnetic field and plasma data used in this study. This study was partially supported by the Chief of Naval Research, and NASA Grants: 80HQTR18T0023, HSWO2R17-0005, 80HQTR19T0062 (CCW).

Conflict of interest The authors indicate that they have no conflicts of interest.

Appendix A: MC Model Formulation

Here we briefly summarize the basic aspects of the MC parameter fitting model (Lepping, Jones, and Burlaga (1990), here referred to as LJB) shown for the reader's convenience (see Appendix A of Lepping et al. (2015) for a more complete description of the model, where the MC is considered to be a special kind of interplanetary flux rope; for general features of such structures see, e.g. Low (1982), Priest (1990), Mulligan, Russell, and Luhmann (1998), Hu and Sonnerup (2001, 2002), Marubashi (2002) and Berdichevsky, Lepping, and Farrugia (2003)). Specifically the MC model used is the static, constant-α, force-free, cylindrically symmetric configuration model (Goldstein, 1983; Burlaga, 1988), given by

$$\nabla^2 \boldsymbol{B} = -\alpha^2 \boldsymbol{B}, \tag{7}$$

where it is assumed that $\boldsymbol{J} = \alpha \boldsymbol{B}$ (this and Equation 7 are given in the international system of units). The Lundquist (1950) solution of Equation 7 yields a Bessel-function (J_0,J_1) formulation for the magnetic field, in terms of axial (A), tangential (T), and radial (R) cylindrical components, by the following:

$$B_{\rm A} = B_0 {\rm J}_0(\alpha r), \quad B_{\rm T} = B_0 H {\rm J}_1(\alpha r), \quad \text{and} \quad B_{\rm R} = 0, \tag{8}$$

where H is the handedness of the field twist, i.e. right-handed (R where $H = +1$) or left-handed (L where $H = -1$). It is also important to recognize that we assume that the flux rope boundary is where the axial field first vanishes. Hence, the seven independent MC fit parameters to be estimated by the model, as employed by our approach are:

B_0, the axial field intensity;
H, the handedness of the field twist (as $+1.0$ for right-handed or -1.0 for left-handed);
R_0, the radius of the MC in AU (usually presented as $2R_0$, the diameter); when $B_{\rm A}$ first goes to zero (as r goes from zero to infinity in $J_0(\alpha r)$) that r is defined as R_0.
$\phi_{\rm A}$, $\theta_{\rm A}$, the longitude and latitude, respectively, of the MC axis (GSE coordinates);
t_0, the center time (i.e. the closest approach time); and
Y_0, the closest approach distance (often called the impact parameter) and sometimes given as a fraction of R_0 (i.e. as $CA = Y_0/R_0$) or as a percentage of R_0. When formulated this way CA becomes one of the fit parameters, and then Y_0 no longer is.

To these parameters we add

τ, the duration of the MC, i.e. the time the spacecraft spends within the MC which is an observable.

We compare t_0 and $\tau/2$ by defining an asymmetry factor (asf) by

$$\text{asf} = |(1 - 2t_0/\tau)| \times 100\%. \tag{9}$$

This equation is designated as Equation [5] in the appendix of Lepping et al. (2015). For the next six equations this style of designation will be used for reference to that paper. Note that ideally $\tau/2$ and t_0 should be equal giving an asf of 0.0%, which in practice rarely occurs. Also what we call quality (Q_0) of the MC parameter fitting depends on many factors as well as on asf and $|\chi_R|$, which is the square root of the reduced chi-squared of the MC fit. See Appendix A of Lepping et al. (2006), which quantitatively prescribes the quality. Q_0 can be 1(excellent), 2(good/fair), or 3(poor) – see Appendix C. Other MC quantities of interest in this study and their definitions are listed in the footnotes of Table 1. The first three listed below, the higher order quantities, arise directly from the Lepping, Jones, and Burlaga (1990) model (also see, e.g., Lepping et al., 2006):

$$\text{axial current density, } J_0 = 2.40 B_0/R_0; \quad \text{see Equation [6]}, \tag{10}$$

$$\text{axial magnetic flux, } \Phi_0 = 1.36 B_0 R_0^2; \quad \text{see Equation [7]}, \tag{11}$$

$$\text{total axial current, } I_T = 3.88 B_0 R_0; \quad \text{see Equation [8]}. \tag{12}$$

To compare the model estimate of the MC radius (R_0), with an estimate of the radius (called R_T) based on the duration (τ), average MC speed (V_{MC}), the closest approach distance (Y_0), and cone angle (β_{CA}) we have from simple geometrical considerations

$$R_T = [Y_0^2 + [(\tau V_{MC}/2)(\sin\beta_{CA})]^2]^{1/2}; \quad \text{see Equation [9]}, \tag{13}$$

where the cone angle is that angle between the MC axis and the vector toward the Sun with vertex at the measuring spacecraft, i.e.

$$\beta_{CA} = \cos^{-1}|(\cos\phi_A \cos\theta_A)|; \quad \text{see Equation [10]}. \tag{14}$$

The two estimates of the radius, R_T and R_0, are checked to see how well they compare. To do this we define a quantity called Check by

$$\text{Check} = (R_T - R_0)/R_0; \quad \text{see Equation [11]}. \tag{15}$$

Check is usually given as a percentage. Small Checks are good cases and large ones are poor cases.

This model yields a magnetic field intensity that is given simply by

$$B_M = |\boldsymbol{B}_M| = B_0[(J_0(R))^2 + (J_1(R))^2]^{1/2}, \tag{16}$$

as seen by Equations 8, where the subscript M refers to the modeled field. In our case R is given by

$$R = \alpha R_0[(CA)^2 + (Z/R_0)^2]^{1/2}, \tag{17}$$

where Z is the distance along the $\mathbf{Z}_{Cl}$-axis in magnetic cloud (Cl) coordinates and $\alpha R_0 = 2.40$ (see Lepping et al., 2006). See Figure 2 and Appendix B for the definition of the Cl system. Ideally then, $\langle B_X\rangle_{Cl}$ (i.e. the average of B_X in Cl coordinates, $B_{X,Cl}$) should always be positive, and ideally $\langle B_Y\rangle_{Cl}$ should be zero (or be nearly zero in practice, for a good case), because of the fundamental field structure of the force-free model (solutions given by Equations 8) and the definition of the Cl coordinate system. Equation 17 can be presented as

$$R = 2.40[(CA)^2 + u^2(1 - (CA)^2)]^{1/2}, \tag{18}$$

where $|u|$ ($\equiv |Z/Z_0|$, and Z_0 is on the MC boundary) is a relative path length of the observing spacecraft through the MC, as shown by Equation 9 in Lepping, Berdichevsky, and Wu (2017). Note that the range of u is 0 to +1, and when thought of as percent of duration it is given by

$$U(\%) = (Z/Z_0 + 1.0) \times 50\%, \tag{19}$$

where $Z/Z_0 = -1.0$ to $+1.0$, and then $U(\%) = 0\%$ to 100%, respectively. We remind the reader that u is measured along the $\mathbf{Z}_{\rm Cl}$-axis in Cl coordinates (see Figure 2).

It is necessary to consider the handedness (H) along with the Type (see Lepping et al., 2006) to give a more complete characterization of the profile a MC, so we define what we call the State (S) of the MC defined by

$$S = \text{Category} \times H, \tag{20}$$

where H is +1 (right-handed) or −1 (left-handed), and where Category means the Type-category (see Table 5) which takes on one of these numbers: 1, 2, 3, 4, 5, 11, 12, 13, 14, or 15.

Appendix B: Magnetic Cloud (Cl) Coordinate System

In the Cl system the $\mathbf{X}_{\rm Cl}$-axis is along the MC axis, positive in the direction of the positive polarity of the axial magnetic field, the $\mathbf{Z}_{\rm Cl}$-axis passes through the MC axis and is aligned with the projection of the trajectory of the spacecraft (relative to the MC velocity, which is approximately aligned with the $\mathbf{X}_{\rm GSE}$-axis) onto the cross-section of the MC, and $\mathbf{Y}_{\rm Cl} = \mathbf{Z}_{\rm Cl} \times \mathbf{X}_{\rm Cl}$. See Figure 2 which shows the circular cross-section of an ideal MC and the projection of the spacecraft path onto the cross-section in Cl coordinates, and see the Wind/MFI Website https://wind.gsfc.nasa.gov/mfi/ecliptic.html for further discussion and derivation of the coordinate transformation from GSE coordinates to Cl coordinates.

Appendix C: Criteria for Estimating the Quality of Magnetic Cloud Fit

We choose to quantify the quality (Q_0) of the model parameter-fitting of a given magnetic cloud into three possibilities, $Q_0 = 1, 2, 3$, for excellent, good/fair, and poor, respectively, given below in terms of magnetic field quantities resulting from use of the MC model (Lepping, Jones and Burlaga, 1990 and see Appendices A and B). However, for the sake of compactness we often refer to quality as a measure of the MC per se, where it is understood that it is mainly the quality of the MC parameter-fitting that is being estimated.

We first describe the characteristics of those MCs that fall into the $Q_0 = 3$ (poor) category. This category arises from satisfying any one of the following $Q_0 = 3$ criteria: $|\text{Check}| \geq 55\%$, $|CA| \geq 97\%$, $\langle B_{\rm X}\rangle_{\rm Cl} \leq -1.5$ nT, either the f-flag or the F-flag = NOT OK, diameter ≥ 0.45 AU, asf $\geq 40\%$, cone angle ($\beta_{\rm CA}$) $\leq 25^\circ$ or $\beta_{\rm CA} \geq 155^\circ$, or $\chi_{\rm R} \geq 0.215$. Notice that $\chi_{\rm R} = 0.215$ corresponds to a MC field noise level ν of 4.0 nT, according to Lepping, Berdichevsky, and Ferguson (2003, 2004), and this is the highest MC noise level that they found acceptable. The remaining cases, comprising designated $Q_0 = 1$ or 2, are next examined to differentiate the excellent cases ($Q_0 = 1$) from the good/fair ($Q_0 = 2$) ones. The $Q_0 = 1$ cases must satisfy all of the following criteria: $|\text{Check}| \leq 20\%$, $|\langle B_{\rm Y}\rangle_{\rm Cl}| \leq 3.0$ nT, asf $\leq 30\%$, $45^\circ \leq \beta_{\rm CA} \leq 135^\circ$, and $\chi_{\rm R} \leq 0.165$. These are the $Q_0 = 1$ set. Notice that

$\chi_R = 0.165$ corresponds to a MC field noise level ν of 3.0 nT, according to Lepping, Berdichevsky, and Ferguson (2003, 2004). The remaining cases within set 1, 2, i.e. those not satisfying the $Q_0 = 1$ criteria, are put into category $Q_0 = 2$.

There are many ways that a MC can achieve a $Q_0 = 3$ quality, so there is no *typical* $Q_0 = 3$ MC. However, χ_R and asf are usually the most important parameters in judging MC quality. The quality criteria (meaning for all $Q_0 = 1, 2, 3$) were derived from our experience in the application of the Lepping, Jones, and Burlaga (1990) model and partly from a desire to be consistent with the results of the error study by Lepping, Berdichevsky, and Ferguson (2003, 2004). The present criteria used in assessing quality consistently represent a distinct improvement over earlier attempts which were mainly visual inspections. It should be stressed that, by our criteria (magnetic field quantities only), a MC may well satisfy the original Burlaga et al. (1981) definition of a MC and still not have good flux rope structure by the Lepping, Jones and Burlaga (1990) model, and therefore not qualify for a Q_0 of 1 or 2.

References

Berdichevsky, D.B.: 2013, *Solar Phys.* DOI.

Berdichevsky, D., Bougeret, J.-L., Delaboudiniere, J.-P., Fox, N., Kaiser, M., Lepping, R., Michels, D., Plunkett, S., Reames, D., Reiner, M., Richardson, I., Rostoker, G., Steinberg, J., Thompson, B., Von Rosenvinge, T.: 1998, *Geophys. Res. Lett.* **25**, 2473.

Berdichevsky, D.B., Lepping, R.P., Farrugia, C.J.: 2003, *Phys. Rev. E* **67**(036405), 1.

Berdichevsky, D.B., Richardson, I.G., Lepping, R.P., Martin, S.F.: 2005, *J. Geophys. Res.* **110**(A09105), 1. DOI.

Bothmer, V., Rust, D.M.: 1997, In: Crooker, N., Joselyn, J., Feynman, J. (eds.) *Geophys. Monogr. Ser.* **99**, Am. Geophys. Union, Washington, 139.

Burlaga, L.F.: 1988, *J. Geophys. Res.* **93**, 7217.

Burlaga, L.F.: 1995, *Interplanetary Magnetohydrodynamics*, Oxford University Press, New York, 89.

Burlaga, L.F., Sittler, E.C. Jr., Mariani, F., Schwenn, R.: 1981, *J. Geophys. Res.* **86**, 6673.

Collier, M.R., Lepping, R.P., Berdichevsky, D.B.: 2005, A statistical study of interplanetary shocks and pressure pulses internal to magnetic clouds. NASA-GSFC internal document.

Dryer, M.: 1994, *Space Sci. Rev.* **67**, 363.

Goldstein, H.: 1983, In: Neugebauer, M. (ed.) *Solar Wind Five*, *NASA Conf. Publ.* **2280**, 731.

Hidalgo, M.A., Nieves-Chinchilla, T., Cid, C.: 2002, *Geophys. Res. Lett.* **29**, 1637. DOI.

Hu, Q., Sonnerup, U.O.: 2001, *Geophys. Res. Lett.* **28**, 467.

Hu, Q., Sonnerup, U.O.: 2002, *J. Geophys. Res.* **107**(A7), 1142. DOI.

Klein, L., Burlaga, L.F.: 1982, *J. Geophys. Res.* **87**, 613.

Lepping, R.P., Berdichevsky, D., Szabo, A., Lazarus, A.J., Thompson, B.J.: 2002, In: Lyu, L.-H. (ed.) *Proceedings of the COSPAR Colloquium in Pacific Green Bay, Taiwan*, *Space Weather Study Using Multipoint Techniques*, Pergamon, Elmsford 87.

Lepping, R.P., Berdichevsky, D.B., Ferguson, T.: 2003, *J. Geophys. Res.* **108**, 1356. DOI.

Lepping, R.P., Berdichevsky, D.B., Ferguson, T.: 2004, *J. Geophys. Res.* **109**, A07101. DOI.

Lepping, R.P., Jones, J., Burlaga, L.F.: 1990, *J. Geophys. Res.* **95**, 11957.

Lepping, R.P., Wu, C.-C., Berdichevsky, D.B.: 2005, *Ann. Geophys.* **23**, 2687. Sref-ID: 1432-0576/ag/2005-23–1432-0576/ag/2005-2687.

Lepping, R.P., Berdichevsky, D.B., Wu, C.-C., Szabo, A., Narock, T., Mariani, F., Lazarus, A.J., Quivers, A.J.: 2006, *Ann. Geophys.* **24**, 215. Sref-ID: 1432-0576/ag/2006-24–1432-0576/ag/2006-215.

Lepping, R.P., Wu, C.-C., Berdichevsky, D.B., Szabo, A.: 2011, *Solar Phys.* **274**, 345. DOI.

Lepping, R.P., Wu, C.-C., Berdichevsky, D.B., Szabo, A.: 2015, *Solar Phys.* **290**, 2265. DOI.

Lepping, R.P., Berdichevsky, D.B., Wu, C.-C.: 2017, *Solar Phys.* **292**(2), 27. DOI.

Lepping, R.P., Wu, C.-C., Berdichevsky, D.B., Szabo, A.: 2018a, *Solar Phys.* **293**, 65. DOI.

Lepping, R.P., Wu, C.-C., Berdichevsky, D.B., Kay, C.: 2018b, *Solar Phys.* **293**, 162. DOI.

Li, Y., Luhmann, J.G., Lynch, B.J.: 2018, *Solar Phys.* **293**, 135. DOI.

Low, B.C.: 1982, *Rev. Geophys.* **20**(1), 145. DOI.

Lundquist, S.: 1950, *Ark. Fys.* **2**, 361.

Marubashi, K.: 1997, In: Crooker, N., Joselyn, J., Feynman, J. (eds.) *Geophys. Monogr. Ser.* **99**, Am. Geophys. Union, Washington, 147.
Marubashi, K.: 2002, *J. Commun. Res. Lab.* **48**(3), 41.
Marubashi, K., Lepping, R.P.: 2007, *Ann. Geophys.* **25**, 2453. www.ann-geophys.net/25/2453/2007/.
Mulligan, T., Russell, C.T., Luhmann, J.G.: 1998, *Geophys. Res. Lett.* **25**, 2959. DOI.
Nieves-Chinchilla, T.: 2018, *IEEE Trans. Plasma Sci.* **46**(7), 2379. DOI. 2018.
Nieves-Chinchilla, T., Vourlidas, A., Raymond, J.C., Linton, M.G., Al-haddad, N., Savani, N.P., Szabo, A., Hidalgo, M.A.: 2018a, *Solar Phys.* **293**, 25. DOI.
Nieves-Chinchilla, T., Linton, M.G., Vourlidas, A., Hidalgo, M.A.: 2018b, *Astrophys. J.* **861**, 139. DOI.
Priest, E.: 1990, In: Russell, C.T., Priest, E.R., Lee, L.C. (eds.) *Physics of Magnetic Flux Ropes*, *Geophys. Monogr. Ser.* **58**, Am. Geophys. Union, Washington, 1.
Vandas, M., Romashets, E.: 2017, *Astron. Astrophys.*. DOI.
Vandas, M., Fisher, S., Geranios, A.: 1991, *Planet. Space Sci.* **39**, 1147.
Vandas, M., Romashets, E.P., Watari, S.: 2005, *Planet. Space Sci.* **53**, 19.
Vršnak, B., Amerstorfer, T., Dumbović, M., Leitner, M., Veronig, A.M., Temmer, M., Möstl, C., Amerstorfer, U.V., Farrugia, C.J., Galvin, A.B.: 2019, Heliospheric evolution of magnetic clouds. *Astrophys. J.* **877**, 77. DOI
Wang, Y., Zhou, Z., Shen, C., Liu, R., Wang, S.: 2015, Investigating plasma motion of magnetic clouds at 1 AU through a velocity-modified cylindrical force-free flux rope model. *J. Geophy. Res.* **120**, 1543. DOI.
Wei, F., Liu, R., Fan, Q., Feing, X.: 2003, *J. Geophys. Res.* **108**(A6), 1238.
Wu, C.-C., Lepping, R.P.: 2015, *Solar Phys.* **290**, 1243. DOI.
Wu, C.-C., Lepping, R.P.: 2016, *Solar Phys.* **291**, 265. DOI.
Wu, C.-C., Lepping, R.P., Berdichevsky, D.B., Liou, K.: 2017, *Space Weather* **15**, 517. DOI.
Zhou, Z., Zou, P., Feng, X., Wang, Y., Jiang, C., Song, X.: 2019, *Solar Phys.* **294**, 149. DOI.